TRENDS IN SCIENCES 2026; 23(12): 13852
https://doi.org/10.48048/tis.2026.13852 RESEARCH ARTICLE

Revisiting the Cytotoxicity of Polyelectrolytes as Microparticle Coatings for Enhanced Curcumin Delivery in Cancer Therapy

Surisak Prasarnpun[1], Netsai Sriaksorn[2], Krissana Khoothiam[3], Nares Khamcharoen[4], Chonthida Thephinlap[2], Chutamas Thepmalee[2] and Nittiya Suwannasom[2,*]

[1]*Division of Physiology, School of Medical Sciences, University of Phayao, Phayao 56000, Thailand*
[2]*Division of Biochemistry, School of Medical Sciences, University of Phayao, Phayao 56000, Thailand*
[3]*Division of Microbiology, School of Medical Sciences, University of Phayao, Phayao 56000, Thailand*
[4]*Public Health Program Department, Faculty of Science and Technology, Kamphaeng Phet Rajabhat University, Kam-Phaeng Phet 62000, Thailand*

([*]Corresponding author's e-mail: nittiya.su@up.ac.th)

Received: 17 March 2026, Revised: 31 May 2026, Accepted: 10 June 2026, Published: 20 July 2026

Abstract

As chemotherapeutic delivery agents, polymeric microparticles (MPs) enhance treatment efficacy and selectivity, playing a crucial role in nanomedicine by enabling targeted release, imaging, and improved therapeutic outcomes. In this study, layer-by-layer (LbL) polymer–coated human serum albumin MPs (HSA/PEI/ALG/HSA-MPs) were developed for the delivery of curcumin (CUR) through electrostatic assembly of poly(ethyleneimine) (PEI) and alginate (ALG) on biodegradable HSA MPs. The successful multilayer assembly was confirmed by changes in particle size and zeta potential following sequential deposition of oppositely charged polymers. The cytotoxicity of individual precursors (HSA, PEI, and ALG) was also evaluated. Pure ALG exhibited minimal cytotoxicity, while HSA maintained relatively high cell viability across the tested concentrations. In contrast, pure PEI displayed cytotoxicity at 3.25 μM, with less than 40% cell viability in cancer cells ($p < 0.001$). *In vitro* experiments showed that PEI-containing MPs (PEI/HSA-MPs and PEI/ALG/HSA-MPs) exhibited a concentration-dependent decrease in cell viability in MCF-7 and MDA-MB-231 cells, indicating that PEI-associated cytotoxicity contributed to the formulations. HSA/PEI/ALG/HSA-MPs maintained higher cell viability than PEI/HSA-MPs and PEI/ALG/HSA-MPs across the tested concentrations, demonstrating that the incorporation of PEI into the shell was successful without compromising cell viability. As drug-loaded microcarriers, LBL-CUR-MPs exhibit negligible cytotoxicity toward cells and low hemolyticity (< 5%) against human red blood cells, indicating good biocompatibility and a CUR loading capacity of 26.5%. CUR-loaded LBL-HSA-MPs exhibited higher toxicity than CUR-HSA-MPs but less than CUR alone, suggesting that CUR delivered through LBL-HSA-MPs exerted a more potent antiproliferative activity than CUR-HSA-MPs. These findings indicate that polymer-coated HSA MPs provide a biocompatible and efficient delivery system for CUR, with potential applications in cancer therapy. Taken together, the LBL-HSA-MPs show promising applications in cancer therapy as a drug microcarrier and warrant further investigation, including *in vivo* evaluation.

Keywords: Poly(ethylenimine), Alginate, Polyelectrolytes, Curcumin, Albumin microparticles, Coatings, Cancer therapy

Introduction

Biopolymers are particularly appealing for drug delivery system (DDS) applications due to their renewability, non-toxicity, excellent biological performance, controlled biodegradability, and cost-effectiveness [1]. Polymer-based nanoparticles (NPs) and microparticles (MPs) specifically designed for cancer therapies cover a significant and extensively researched area within nanotechnology [2,3]. The main

advantages reside in their versatility, as their properties can be easily tailored by selecting specific polymer types and preparation methods. This allows precise control over surface characteristics that influence biological interactions, such as drug distribution within the body and the timing of drug release, ensuring targeted and timely drug availability [4,5]. The extensive exploration of albumin-based MPs in recent years has also demonstrated that this biopolymer can play an important role in DDS.

Albumin-based delivery systems offer several advantages due to their natural transport functions. Mechanisms such as hydrophobic attractions, electrostatic interactions, and covalent bindings facilitate drug attachment to the carrier [6]. These systems can be degraded into peptides by naturally occurring enzymes, improving drug stability and enabling accumulation in tumor tissues via the enhanced permeability and retention effect. Developed to improve the delivery of hydrophobic drugs, albumin-based delivery systems exploit their multiple ligand binding sites and cellular interactions, making them a promising approach for drug delivery [7]. Meanwhile, NP albumin-bound (nab)-paclitaxel, with a particle size of about 130 nm, has been designed to maintain the therapeutic benefits of paclitaxel while avoiding the toxicity associated with the polyoxyethylated castor oil in Taxol, significantly reducing allergic reactions and eliminating the need for pretreatment [8,9]. Although clinical trials have shown fewer adverse effects, ongoing research aims to optimize efficacy and address safety concerns related to albumin-based nanocarriers [10,11].

To address these challenges, the interactions between biodegradable cationic and anionic biopolymers that form polyionic hydrogels have been employed. This method not only improves the stability and biocompatibility of the NPs but also enhances cellular uptake. Functionalization via LBL coating enables better interaction with cellular membranes and the activation of internalization pathways, potentially improving therapeutic outcomes [12]. Recent studies have demonstrated that multilayer polymer-coated delivery systems can improve cellular uptake, prolong drug release, and enhance the biocompatibility of anticancer formulations, highlighting the growing interest in layer-by-layer (LbL) surface engineering strategies for cancer drug delivery [13].

A significant advancement in nanotechnology for cancer treatment is the use of functionalized polymers to construct layered MPs. Notable examples include sodium alginate (ALG) and polyethyleneimine (PEI). ALG, a natural polysaccharide polymer, offers the advantages of biocompatibility, non-toxicity, biodegradability, flame retardancy and low cost [14,15]. PEI, a cationic polymer, is a synthetic polymer, synthesized from aziridine by cationic polymerization. It offers a potential gene delivery system due to its high amine content. This high amine content produces a substantial proton-sponge effect, which facilitates the early escape of complexes from endolysosomal compartments [16]. This property makes PEI promising for delivering drugs for cancer therapy, promoting deep penetration in tumor tissues [17].

Additionally, PEI can exert anticancer effects through electrostatic interaction at the cell membrane surface [18]. Nevertheless, cationic MPs, including those made from PEI, are rapidly cleared by the reticuloendothelial system (RES) through formation of complexes with negatively charged cell membranes or serum proteins. Moreover, many cationic nanosystems exhibit relatively high toxicity and lack targeting specificity, limiting their broad clinical applicability. This demands strategies for reversibly shielding their surfaces with biomimetic coatings [19]. Therefore, the conjugation of PEI has been proposed to fabricate albumin-based particles. PEI coating may enhance the biocompatibility and permeability of albumin-based particles. The PEI coating may enhance the biocompatibility and permeability of albumin-based particles while reducing the cell-induced toxicity of PEI by decreasing the density and the significant positive surface charge of the polymer responsible for its toxic effects.

In our previous study, we investigated the co-encapsulation of albumin and CUR produced through Co-precipitation Crosslinking Dissolution (CCD)-technique [20]. CUR-encapsulated albumin MPs (CUR-HSA-MPs) were advantageous in terms of *in vitro* cytotoxicity against human breast adenocarcinoma (MCF-7) and human hepatocellular carcinoma (Huh-7) cell lines; however, this effect was more pronounced for free CUR. Because CUR had very low water solubility, this work aims to improve the therapeutic performance of CUR-loaded MPs by applying an LbL polymer

coating of poly(ethyleneimine) (PEI) and alginate (ALG).

In contrast to the previously reported CUR-HSA-MPs system, the present study developed LbL polymer–coated HSA MPs (LbL-HSA-MPs) through sequential electrostatic assembly of cationic PEI and anionic ALG layers. This multilayer surface engineering strategy was designed to improve cellular interaction, biocompatibility, and antiproliferative activity while partially reducing the inherent cytotoxicity of free PEI. In addition, this study investigates the cytotoxic effects of pure polymers and their corresponding multilayer-coated formulations on cell viability. The LbL-HSA MP system may provide a biocompatible platform for improved CUR delivery in cancer therapy.

Materials and methods

Materials

Poly (ethyleneimine) solution (PEI, average Mn ~60,000 by GPC, average Mw ~750,000 by LS, 50 wt.% in H_2O), human serum albumin solution (100 g/L HSA in 0.14 M NaCl), sodium borohydride ($NaBH_4$), and manganese (II) chloride tetrahydrate ($MnCl_2 \cdot 4H_2O$) were obtained from Sigma-Aldrich (Munich, Germany). Alginic acid sodium salt (molecular weight: 30,0000 - 350,000 g/mol) was purchased from Carl Roth GmbH (Karlsruhe, Germany). 25% Glutaraldehyde solution in water (GA) and anhydrous sodium carbonate (Na_2CO_3) were purchased from Merck KGaA (Darmstadt, Germany). Dimethyl sulfoxide (DMSO) was supplied by Panreac Applichem® (Barcelona, Spain). Fluorescein isothiocyanate (FITC) was obtained from Biochrom GmbH (Berlin, Germany). Ethylene diamine tetra-acetic acid (EDTA) disodium salt dehydrate, sodium hydroxide (NaOH) and sodium chloride (NaCl) were obtained from HiMedia Laboratories Pvt. Ltd. (Mumbai, India).

Preparation of albumin MPd (HSA-MPs) loaded with CUR

HSA-MPs were synthesized through a modified CCD technique, as shown in **Figure 1(a)** [21]. Briefly, Na_2CO_3 (0.25 M) and $MnCl_2$ (0.25 M) containing 0.5% HSA solution were mixed in a beaker under magnetic stirring for 30 s at room temperature (RT). The pellets ($MnCO_3$-HSA-MPs) were then separated and washed by centrifugation twice at 6,000 × g for 3 min. An aliquot of an 8% volume concentration of $MnCO_3$-HSA-MPs suspension was then incubated with CUR at a concentration of 1 mg/mL in DMSO for 1 h at RT and protected from light. After incubation, the mixture was centrifuged and washed three times with distilled (DI) water at 6,000 × g for 10 min. The obtained particles were resuspended and crosslinked with a 0.08% GA solution in 0.9% NaCl, then agitated for 1 h, while shielded from direct light. Then, 0.5 mL of solution containing 15 mg/mL $NaBH_4$ in 0.1 M NaOH was added and the mixture was stirred for 30 min at RT. Subsequently, 0.25 M EDTA was added to dissolve the carbonate core, and the mixture was incubated for another 30 min. The final particles were washed in DI water (6,000 × g for 10 min). This washing step was repeated three times, and the particles were resuspended in PBS (pH 7.4) and stored at 2 - 8 °C until use. The obtained particles are referred to as CUR-HSA-MPs.

The control particles, HSA-MPs, were prepared by following the same procedure without the adsorption of CUR.

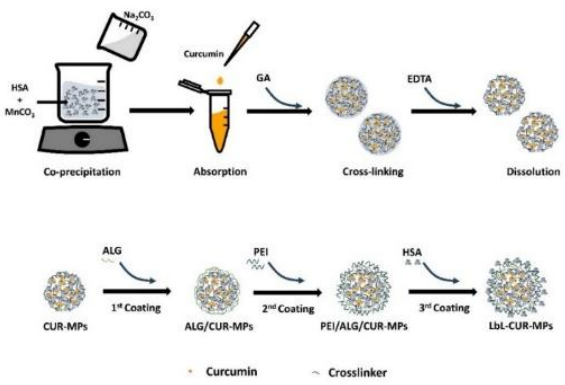


Figure 1 Schematic of (a) CUR-HSA-MP preparation via co-precipitation, CUR loading, cross-linking, and core removal, (b) followed by layer-by-layer coating with ALG, PEI, and HSA (LbL-CUR-MPs).

Layering procedure

The multilayer shell was formed via sequential electrostatic adsorption of oppositely charged cationic PEI and anionic ALG layers onto the negatively charged HSA MP surface, as shown in **Figure 1(b)**. First, HSA-MPs were incubated with 2 mg/mL alginate for 15 min at RT. ALG/HSA-MPs were then centrifuged three times at 6,000 × g for 10 min each to complete the washing step. Second, the negatively charged particles were dispersed in 0.9% NaCl and incubated with a 2 mg/mL PEI solution for 15 to impart a positive charge (reducing the negative charge). Afterward, the PEI/ALG/HSA-MPs were washed three times with DI water and resuspended in 0.9% NaCl. Finally, the bilayer-deposited MPs were incubated in a 2% HSA solution for 15 min to stabilize them. After three DI water washes, the supernatant was removed, and the final sediment of HSA/PEI/ALG/HSA-MPs was suspended in 0.9% NaCl, then stored at 4 °C for further use. These HSA/ PEI/ALG/HSA-MPs are hereafter referred to as LbL-HSA-MPs.

Drug loading determination

The quantity of CUR in the MPs was measured at 435 nm using an Optizen Pop UV/Vis spectrophotometer (Mecasys Co., Ltd., Daejeon, South Korea). The encapsulation efficiency (EE) was calculated using the following Eq. (1);

$$\%EE = \left(\text{Amount of CUR present}\frac{\text{MPs}}{\text{Amount}}\text{of CUR used}\right) \times 100\% \quad (1)$$

Characterization of albumin MPs

Size and zeta potential: The size and zeta potential of the obtained particles were measured using a Zetasizer instrument (Malvern Instruments Ltd., Malvern, UK) at 25 °C. The microparticles are dispersed in PBS pH 7.4 under mild sonication to avoid the formation of large aggregates Aliquots of the solution were placed in a plastic cuvette for particle size measurement and the zeta cell for zeta potential measurement.

Chemical characteristics: To collect the Fourier transform infrared spectrometer (FTIR) spectra of HSA, ALG, PEI, and LBL-HSA-MPs, a NICOLET iS5 FTIR spectrometer (Thermo Scientific, Waltham, MA, USA) was employed. The FTIR spectra ranged from 400 to 4,000 cm^{-1} with a resolution of 4 cm^{-1}.

Morphology: Samples were imaged using a scanning electron microscope (LV-Scanning Electron Microscope, JSM 5910 LV, Tokyo, Japan). A drop of the particle suspension was applied to a glass slide, allowed to dry overnight at RT, and sputtered with gold. SEM images were conducted at an operating voltage of 15 kV. The average particle size and size distribution were obtained using Image J software (NIH, Bethesda, MD, USA) and Origin 10.0 software (OriginLab, Northampton, MA, USA).

Cell culture

Human breast cancer cells (MCF-7 [#HTB-22; ATCC] and MDA-MB-231 [#HTB-26; ATCC]) and osteosarcoma cells (MG-63 cell [#CRL-1427; ATCC]) were cultured in Dulbecco's modified Eagle's medium (DMEM; Gibco)/F12 supplemented with 10% (v/v) fetal bovine serum (FBS; Gibco), and 1 × antibiotic and antimycotic solution (Gibco). All cell lines at passages 5 - 10 were used in this study and maintained at 37 °C in a humidified atmosphere containing 5% CO_2.

Cytotoxicity of polymers and polymers-coated MPs

Cells were plated at a density of 5×10^4 cells per well in 96-well plates. The concentrations of pure polymers ranged from 3.125 to 50 μM, and polyelectrolyte MPs ranged from 1.56 to 50 mg/mL. Free CUR was used as a positive control, whereas untreated cells served as the negative control. The samples were added to each cell line after 24 h of cell cultivation. The metabolic activity of the cells was measured using the 3-(4,5-dimethylthiazol-2-yl)-2,5-diphenyltetrazolium bromide (MTT) test after cultivation with samples for 24 and 48 h. For the MTT assay, 10 μL of the stock MTT solution (5 mg/mL in PBS) was added to each well, and the plates were incubated for 2 h at 37 °C in a 5% CO_2 humidified atmosphere.

The MTT solution was removed, and the crystal formazan was dissolved with 100 μL of DMSO per well, then measured using a microplate reader at 570 nm.

Uptake of polyelectrolyte multilayer MPs

The HSA-MPs and CUR-HSA-MPs (8%) were incubated with freshly prepared FITC at a ratio of 9:1 at RT for 1 h in the dark. The labeled particles were then cleaned three times with DI water to remove free FITC and finally resuspended in PBS. HPA-FITC-HSA-MPs and HPA-FITC-CUR-HSA-MPs were prepared by layering FITC-HSA-MPs and FITC-CUR-HSA-MPs with ALG and PEI, as described in the layering procedure given in Section 2.3.

MCF-7 cells were plated into 8-well plates at a density of 2.5×10^4 cells per well. After 24 h of cultivation, the medium was removed, and fresh medium containing polyelectrolyte MPs at 12.5 mg/mL was added. The plates were incubated for 4 h at 37 °C in a 5% CO_2-humidified atmosphere. The cells were then washed with PBS (pH 7.4) and fixed with PBS containing 10% paraformaldehyde for 10 min on ice, followed by three washes with PBS (pH 7.4). The cellular uptake of polyelectrolyte MPs was estimated using an AX/AX R Nikon CLSM (Tokyo, Japan).

Hemolysis tests

All experimental procedures were conducted with the approval of the University of Phayao Ethics Human Committee (UP-HEC 1.2/089/66). Written informed consent was obtained from all blood donors. To assess the hemolysis ratio (HR), fresh blood was drawn from healthy volunteers into BD Vacutainer tubes containing lithium heparin. The samples were centrifuged at 3,000 × g for 5 min to isolate red blood cells (RBCs), which were then washed with PBS (pH 7.4) and resuspended in sterile isotonic PBS at 2% (v/v).

A 0.2 mL aliquot of the RBC suspension was mixed with various samples in 0.8 mL PBS. Controls included 0.2 mL of RBC suspension mixed with 0.8 mL of deionized water (positive) and PBS (negative). After gentle mixing, the samples were incubated at 37 °C for 4 h, shaking every 30 min. Following incubation, samples were centrifuged, and 150 µL of supernatant was transferred in triplicate to a 96-well plate for absorbance measurement at 570 nm using a Cytation 5 Cell Imaging Multi-Mode Reader. Hemolysis percentages (HP) were calculated using the following formula.

$$\%HP = \frac{\text{absorbance of sample}-\text{absorbance of negative control}}{\text{absorbance of positive control}-\text{absorbance of negative control}} \quad (2)$$

Statistics

All experiments were performed at least three times. Statistical analysis was performed using GraphPad Prism 8 (GraphPad Software, La Jolla, CA). All data were analyzed using two-way analysis of variance (ANOVA) and Tukey's multiple comparison test. Values were considered statistically significant at a threshold of $p < 0.05$.

Results and discussion

Cytotoxicity Activity of Its Precursors

A versatile strategy for modifying the toxicity of PEI is the incorporation of biodegradable polymers [22,23]. To investigate whether the incorporation of biodegradable ALG and HSA improves the biocompatibility of PEI, the cytotoxicity of PEI, ALG, and HSA in human breast cancer cell lines (MCF-7 and MDA-MB-231 cells) was determined by MTT assay. There was no appearance difference in the cytotoxicity trends observed among the two cell lines. As shown in **Figures 2(a) - 2(d)** ALG exhibited minimal cytotoxicity over the tested concentration range. HSA also maintained relatively high cell viability (> 80%) up to 25 µM, although MDA-MB-231 cells showed a statistically significant reduction in viability at higher concentrations. In contrast, pure PEI began to exhibit cytotoxicity at 3.125 µM ($p < 0.001$): Fewer than 40% of cells were viable in the presence of PEI.

In addition, we explored the cytotoxicity of PEI using osteosarcoma MG-63 cells. As seen in **Figures 2(e) - 2(f)**, PEI exhibited similar toxicity across different cell lines, highlighting its broad toxicity. **Figure 2** also showed that cell inhibition was time-dependent for pure PEI treatment. Biocompatibility depends on the properties of PEI, such as its molecular weight and form (linear or branched), as well as the experimental cell type. In accordance with previous research, this review revealed the biocompatibility and bifunctionality of PEI, particularly those conducted using human corneal epithelial cells (HCE) [24] and cancer cells [25]. The branched PEI exhibited higher toxicity than the linear PEI in treated cells [26].

The toxicity also increased with higher molecular weights of cationic polymer due to excessive accumulation of cationic polymer on the anionic cell membrane [27]. The studies by Naumenko *et al*. [28] and Wang *et al*. [29] consistent with our findings that this PEI is clearly not biocompatible when used as a precursor base layer for polyelectrolyte coatings.

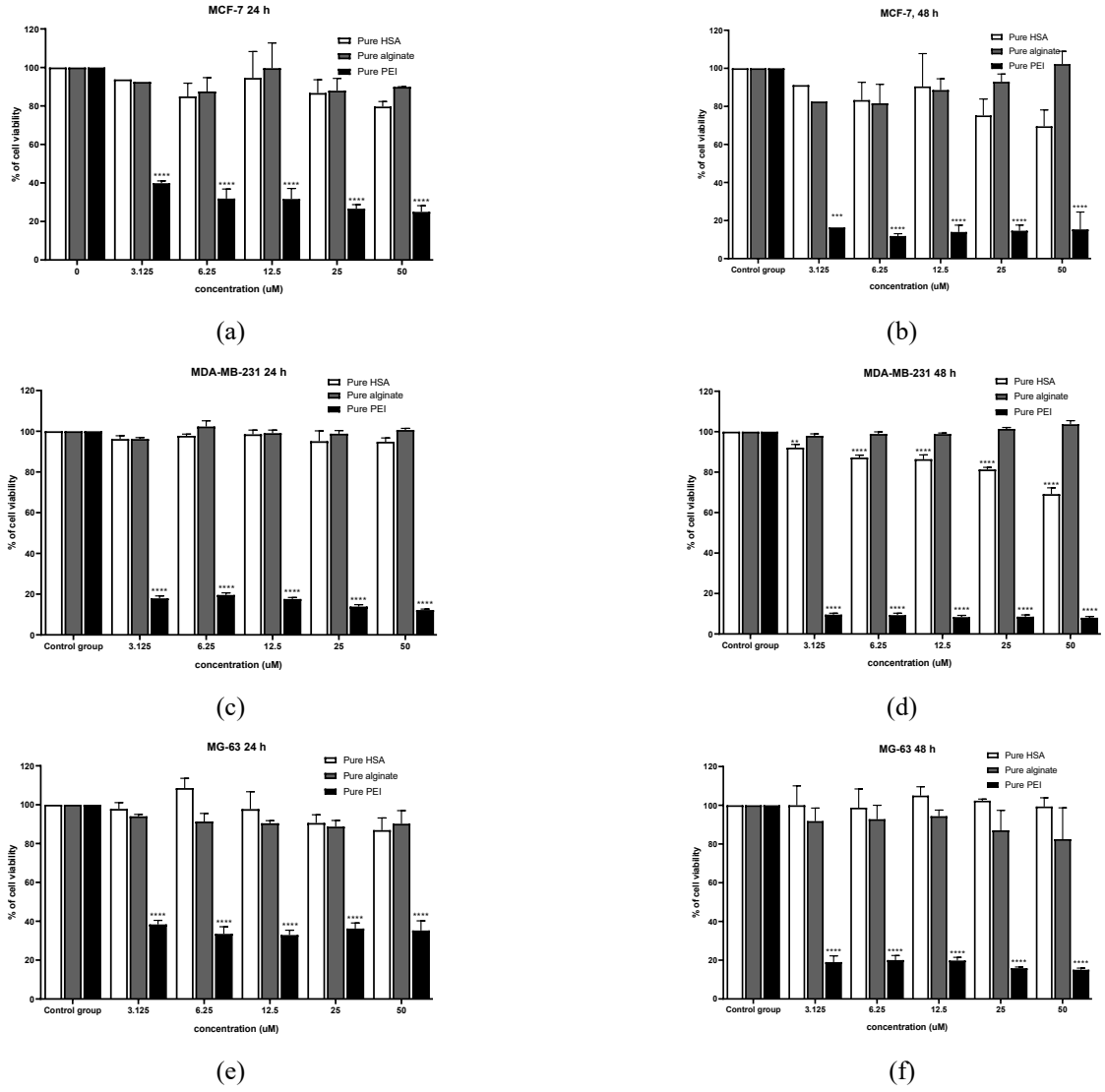


Figure 2 Cytotoxicity effect of the precursors on (a,b) MCF-7 cells, (c,d) MDA-MB-231, and (e,f) MG-63 at 24 and 48 h incubation (n = 3). Mean ± standard error of the mean for the triplicate wells are reported. Statistically significant values (***$p < 0.001$ and ****$p < 0.0001$) were compared with the control group and analyzed by two-way ANOVA with Tukey post-hoc test.

Preparation and Characterization of HSA/ALG/PEI/HSA-MPs (LBL-HSA-MPs)

Layering procedure

The CCD technique used to prepare the HSA MPs is easy and cost-effective [21,30,31]. The resulting particles exhibited consistent size, surface zeta potential, and morphology. The CCD technique involves mixing $MnCl_2$ and Na_2CO_3 in the presence of HSA, encapsulating the HSA within the $MnCO_3$-HSA-MPs. In our previous research, we demonstrated an entrapment efficiency of 55% to 62%, with up to 31.3 ± 1.8 mg of HSA per 5 mg/mL HSA [20]. These parameters remained consistent in this study. GA cross-linking was performed to stabilize the HAS-MPs before applying the polymer surface coating, which also enhances the drug entrapment capacity of the particles.

Preparation of LBL-HSA-MPs involves a multi-step process: i) creating the HSA-MPs core template; ii) applying a negative ALG layer; iii) adding a positive layer of PEI; and iv) incorporating a negative HSA (**Figure 1**). HSA-MPs were fabricated using the CCD technique of $MnCl_2$ and Na_2CO_3 solution in the presence of HSA. The morphologies of LBL-HSA-MPs changed with varying concentrations of ALG and PEI (data not shown). A concentration of 5 mg/mL for ALG and PEI was chosen for all subsequent experiments.

Following the washing step to remove unadsorbed ALG, PEI was adsorbed as the first positive layer through electrostatic interactions by adding the MPs to a PEI solution. Then, ALG was adsorbed to enhance the interaction strength of PEI for the subsequent layer. Attractive interactions between proteins and polysaccharides result mainly from electrostatic interactions between negatively charged polysaccharide groups and positively charged protein groups [32]. Therefore, the sequential deposition of PEI and ALG facilitates the formation of a stable multilayer coating on the HSA microparticle surface.

The process of growing polymer layers on the surface of MPs can be significantly impacted by various experimental factors, particularly the salt concentration [33]. It has been suggested that using covalent process for PEI adsorption can improve the stability of the upper layer [34]. However, our findings suggest that a simple non-covalent deposition may suffice to achieve strong anchorage of PEI on ALG-HSA-MP surfaces.

Determination of size and zeta potential

The surface modification of PEI was confirmed by observing changes in surface potential, as shown in **Table 1**. All samples were dissolved in PBS (pH 7.4) before measurements. The surface potential of the negatively charged HSA-MPs with unmodified ALG (−17.06) became more negatively charged (−17.00 mV) after modification with ALG (ALG/HSA-MPs). The PEI layers were able to neutralize the negative surface potential of the ALG/HSA-MPs (−9.27). Results of zeta potential measurements indicate that the PEI amines were successfully modified through various derivatization reactions. The diameters of the polyelectrolyte MPs increased with more layers, exhibiting a wide size distribution ranging from 1.7 to 4.7 μm, as shown in **Table 1**.

Table 1 Hydrodynamic diameters and zeta potentials of the polyelectrolyte MPs.

Samples	Z- average size (μm)	Zeta potential (mV)
HSA-MPs	1.7 ± 0.03	−17.06 ± 1.14
ALG/HSA-MPs	2.01 ± 0.39	−17.00 ± 0.92
PEI/HSA-MPs	1.6 ± 0.03	−9.27 ± 1.04
PEI/ALG/HSA-MPs	4.7 ± 0.53	−8.03 ± 0.64
LbL-HSA-MPs	3.8 ± 0.16	0.41 ± 0.37

Data are presented as mean ± SD. (n = 3).

The FTIR spectra of pure components (HSA, ALG, and PEI) and related MPs are presented in **Figure 3**. The FTIR spectra of HSA showed characteristic adsorption bands for the amide I (C=O stretching) at 1,650 and amide II (C–N stretching and N–H bending) vibrations at 1,532 cm^{-1}. These bands represent the main vibrational bands in the albumin backbone, contributing to its secondary structure. For ALG, major peaks were observed at 1,596 (C=O bond) and 1,404 cm^{-1}, attributed to the antisymmetric and symmetric stretches of the carboxylate group. A broad band between 3,000 and 3,700 cm^{-1} was observed due to the O-H stretch of the amide group, while peaks in the 1,082 - 1,026 cm^{-1} range correspond to the C-O-C antisymmetric stretch. The FTIR spectrum of PEI displays a broad band at 3,284 - 3,356 cm^{-1} representing N–H stretching vibrations, and peaks at 2,834 - 2,943 cm^{-1} representing aliphatic C–H stretching vibrations. The N–H vibrations of primary and secondary amino groups were observed at 1,559 and 1,457 cm^{-1}, respectively. The band at 1,457 cm^{-1} is also related to the C–H bonds. Additionally, peaks at 1,311 cm^{-1} and within the 1,045 - 1,116 cm^{-1} range were linked to C–N stretching vibrations.

In the spectra of the physical mixture, characteristic peaks similar to those in the spectra of PEI, ALG, and HSA were observed, i.e., 3,278, 2,927 and 1,654 cm^{-1}, confirming the presence of the polymer. However, new peaks also emerged (**Figure 3**).

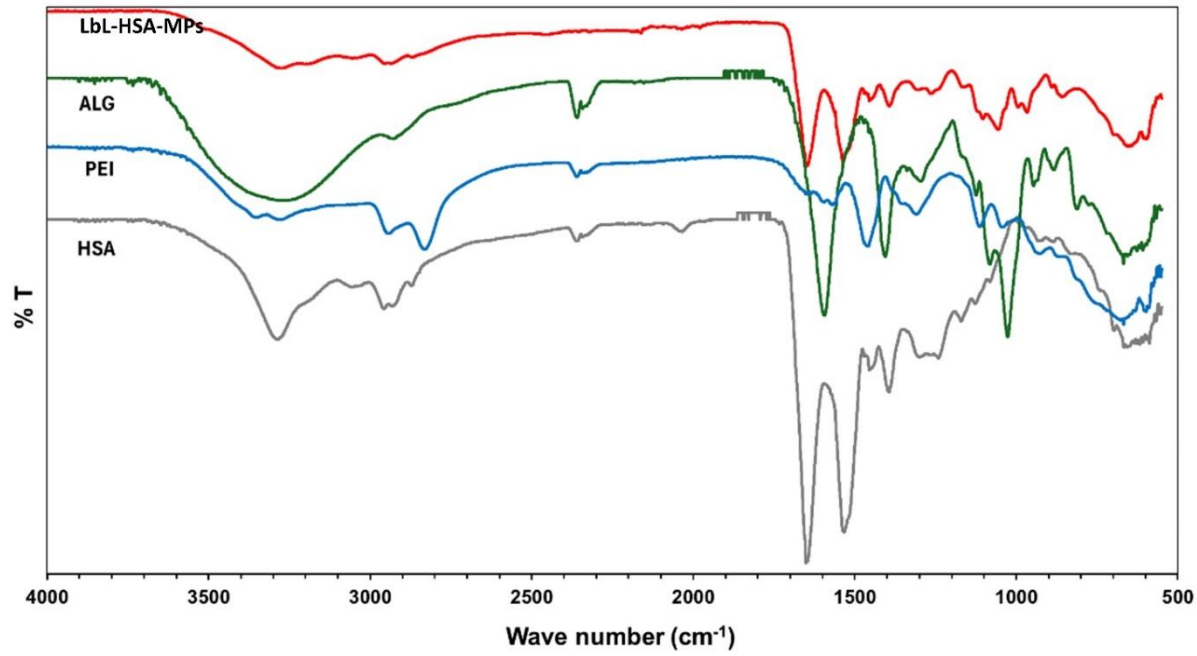


Figure 3 FTIR spectra of HSA, ALG, PEI, and LbL-HSA-MPs.

Morphology

SEM images show that HSA-MPs and ALG/HSA-MPs were peanut-shaped particles with a smooth morphology and a homogenous distribution (**Figures 4(a) - 4(b)**). In contrast, the surfaces of the PEI/ALG/HSA-MPs and LBL-HSA-MPs were relatively uneven (**Figures 4(c) - 4(d)**). The shape and size distribution of the LBL-HSA-MPs differed from that of the template. The LBL-HSA-MPs had a wide particle-size distribution, ranging from several tens to several hundreds of nm. The samples treated with PEI contain small amounts of self-assembled particles, possibly due to an insufficient amount of MP template to increase the mobility of all polymeric chains in the system. The average particle size, calculated using ImageJ from the SEM images, was approximately 0.52 ± 0.093 µm, 0.57 ± 0.12 µm, 0.52 ± 0.18 µm, and 0.2 ± 0.15 µm for HSA-MPs, ALG/HSA-MPs, PEI/ALG/HSA-MPs, and LbL-HSA-MPs, respectively. The particle size distributions are presented as histograms in **Figure 4**. The particle sizes observed by SEM were smaller than those measured by DLS because SEM was performed in the dry state. In contrast, DLS measured the hydrodynamic diameter of particles dispersed in aqueous medium.

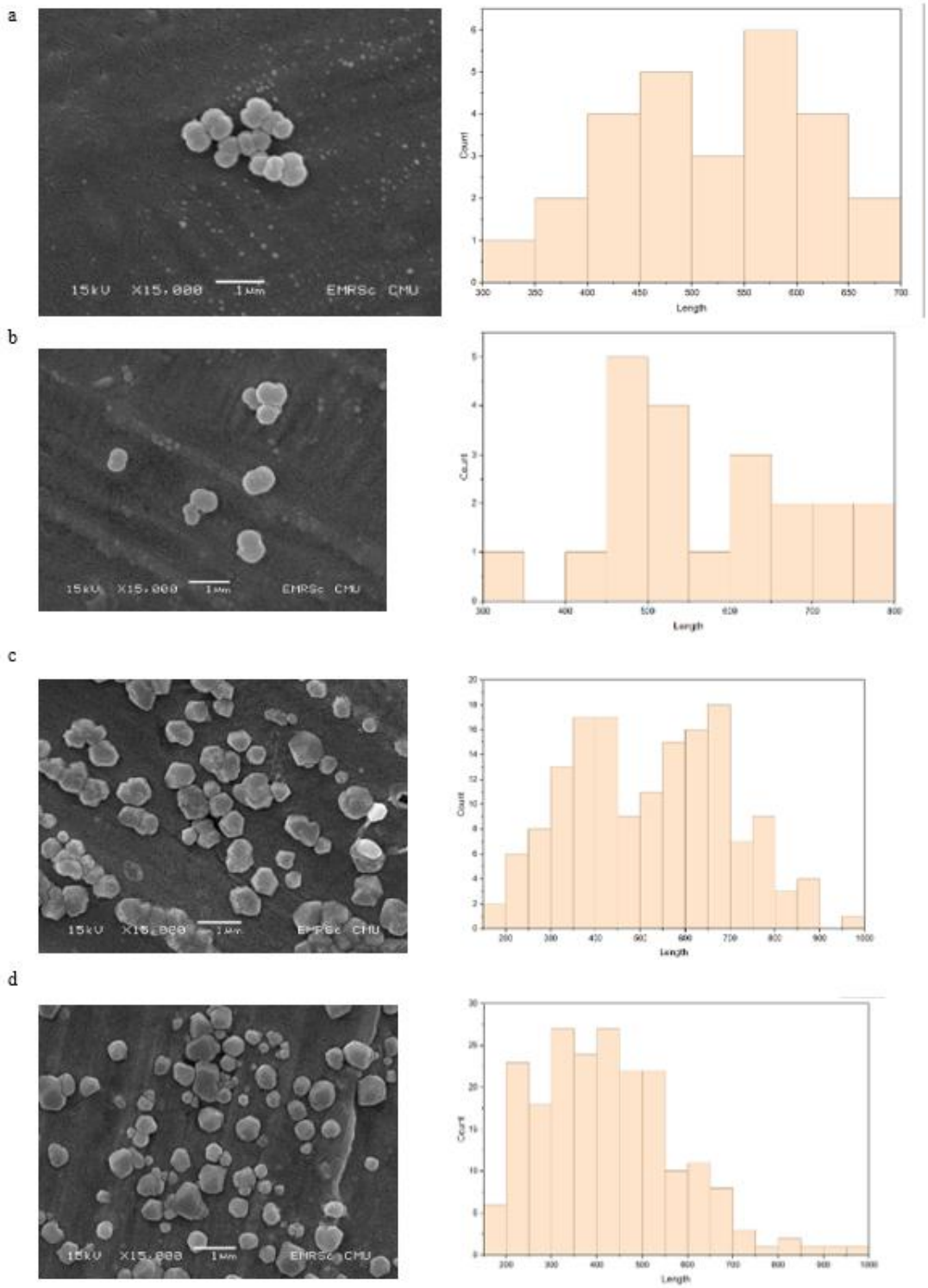


Figure 4 SEM images along with histogram showing grain size distribution of control HSA-MPs, (b) HSA-MPs coated with first ALG layer (ALG/HSA-MPs), (c) HSA-MPs coated with second PEI layer (PEI/ALG/HSA-MPs), and (d) HSA-MPs coated with HSA third layer (LbL-HSA-MPs).

Cytotoxicity activity of polyelectrolyte MPs

Compared with free PEI, coated samples exhibited modified cytotoxicity. As summarized in **Figure 5**, PEI/HSA-MPs showed obvious dosage-dependent cytotoxicity. At the same time, PEI/ALG/HSA-MPs showed a reduction in cell viability, indicating that incorporating ALG into the multilayer shell partially mitigated the inherent toxicity associated with PEI.

Overall, the reduction in cell viability observed in both MCF-7 and MDA-MB-231 cells indicated the concentration-dependent cytotoxic behavior of the PEI-containing MPs.

According to ISO 10993-5 guidelines, materials maintaining cell viability above 80% are generally considered non-cytotoxic. In the present study, HSA-MPs and ALG/HSA-MPs exhibited minimal cytotoxicity at concentrations below 25 mg/mL in both MCF-7 and MDA-MB-231 cells, indicating acceptable biocompatibility. LbL-HSA-MPs also maintained relatively high cell viability compared with PEI/HSA-MPs under the same experimental conditions.

For MCF-7 cells, treatment with HSA-MPs, ALG/HSA-MPs, and LbL-HSA-MPs at a concentration of 25 mg/mL for 48 h resulted in cell viabilities of 84.17 ± 1.53%, 88.51 ± 6.30%, and 66.06 ± 11.68%, respectively. These values were notably higher than those observed for PEI/HSA-MPs (14.17 ± 2.93%) and PEI/ALG/HSA-MPs (68.86 ± 11.00%). Among all tested formulations, the PEI/HSA-MPs treatment exhibited the highest cytotoxicity and the lowest cell viability among the five types of MPs. MP concentrations are expressed in mg/mL throughout this study.

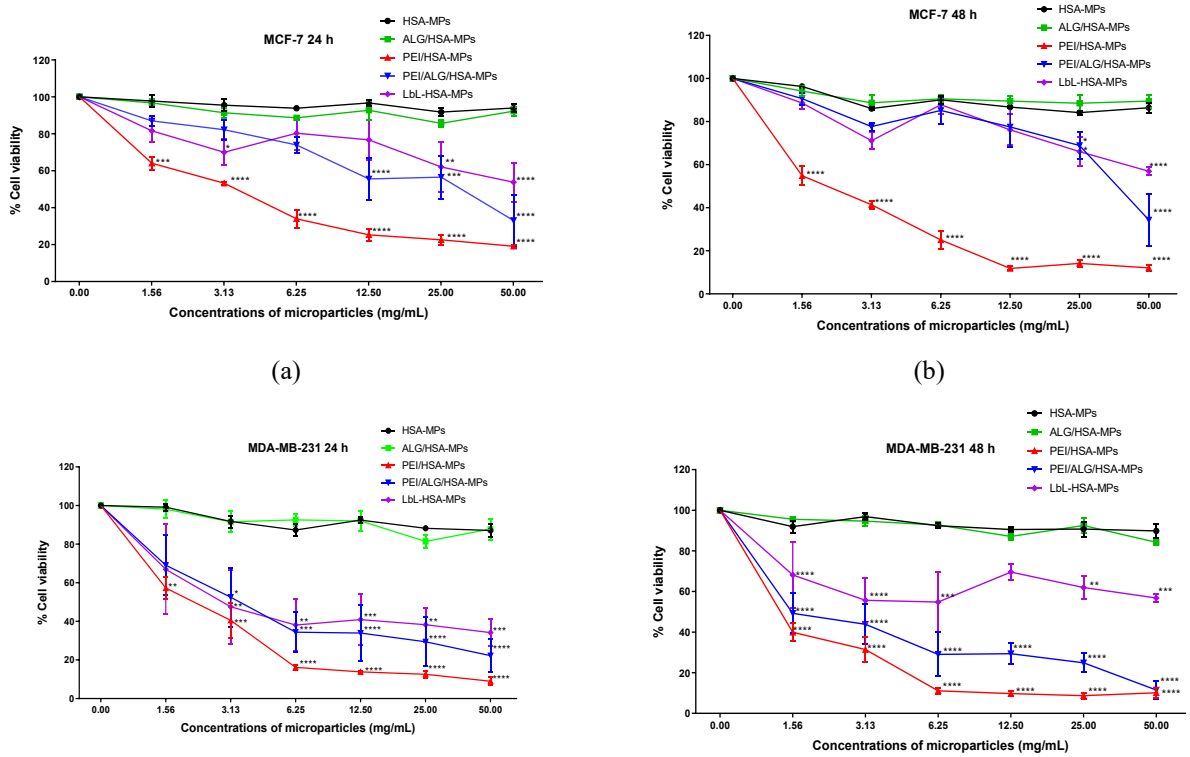


Figure 5 Cytotoxicity effect of HSA-MPs, ALG/HSA-MPs, PEI/HSA-MPs, PEI/ALG/HSA-MPs, and LbL-HSA-MPs toward breast cancer cells. (a) MCF-7 cells after 24 h incubation; (b) MCF-7 cells after 48 h incubation; (c) MDA-MB-231 cells after 24 h incubation; and (d) MDA-MB-231 cells after 48 h incubation. As the dosages ranged from 3.125 to 50 mg/mL, all experiments were performed in triplicate. All data are expressed as mean ± standard error of the mean. Statistically significant values (*$p < 0.05$, **$p < 0.01$, ***$p < 0.001$, and ****$p < 0.0001$) were compared with control group and analyzed by two-way ANOVA with Tukey post-hoc test.

The use of HSA in combination with PEI increased cell viability across all three tested cell types. The cytotoxicity of PEI is primarily attributed to the strong electrostatic interactions between its positively charged sites and the negatively charged cell membranes [35]. The surface charge derived from the PEI segment is a critical factor influencing the cytotoxicity of PEI-based polymers [26]. After modification to neutralize the PEI amines, the positive charges were shielded, significantly improving the

biocompatibility of PEI. The spatial distribution of HSA on the surface of PEI/ALG/HSA-MPs likely reduced or shielded some of the positive charges through electrostatic interaction, decreasing the surface charge [4,36]. Consequently, LBL-HSA-MPs exhibited lower cytotoxicity than PEI/ALG/HSA-MPs, suggesting that HSA has a cytoprotective effect. This supports the hypothesis that the cytotoxicity of PEI is substantially reduced when delivered via NPs, likely due to suppression of its cationic charge in solution [4,37].

Cellular uptake was assessed in MCF-7 cells because they have a high affinity for albumins, which cancer cells absorb at a higher rate due to increased metabolism. The green fluorescent signal from LBL-FITC-HSA-MPs was observed in MCF-7 cells after 4 h of incubation (**Figure 6**), indicating that the MPs were efficiently and continuously endocytosed by cancer cells. By comparing the fluorescence intensities, the cellular uptake in LbL-FITC-HSA-MPs was higher than that in FITC-HSA-MPs. Higher cellular uptake efficiency could be achieved using PEI coating. The PEI conjugate suggests that there might be more contact with PEI carriers on the cell membrane, and consequently, higher cellular uptake efficiency. Indeed, PEI-based systems tend to enter cells through caveolae-mediated endocytosis or micro-pinocytosis [38].

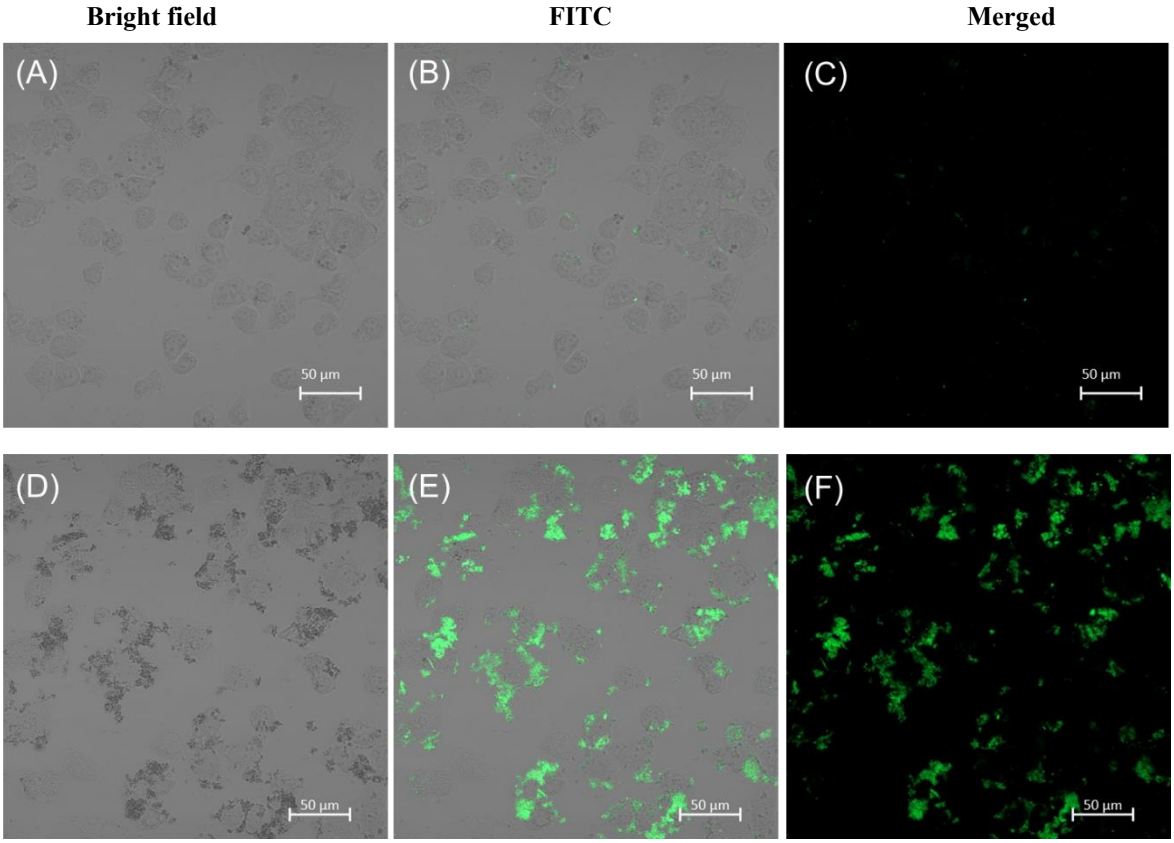


Figure 6 Confocal images demonstrating cellular uptake of (a-c) FITC-HSA MPs and (d-f) LbL-FITC-HSA MPs by MCF-7 cells after 4 h of incubation.

Cytotoxicity activity of polyelectrolyte MPs encapsulated with curcumin

The potential application of LbL-HSA-MPs as a multifunctional carrier for drug delivery was evaluated by loading them with CUR. CUR was loaded onto MPs prior to cross-linking, then dissolved in EDTA. A high loading efficiency of 26.5% was achieved. The PEI coating is likely to hold back drug leakage. The difference in morphology between HSA-MPs and LbL-HSA-MPs might be attributed to the nature of their polymers [25]. The CUR loading capacity obtained in this study (26.5%) was within the range reported for albumin- and polymer-based CUR delivery systems. However, the EE may vary depending on formulation strategy, polymer composition, and preparation conditions [39,40].

To investigate the successful loading of CUR on LbL-HSA-MPs, the fluorescence spectra of LbL-HSA-MPs and LbL- CUR-MPs at the same laser power were studied (**Figures 7(a) - 7(b)**, respectively). Significant fluorescence intensity was observed for CUR after loading LbL-HSA-MPs, indicating successful loading and confirming its interaction with the MPs.

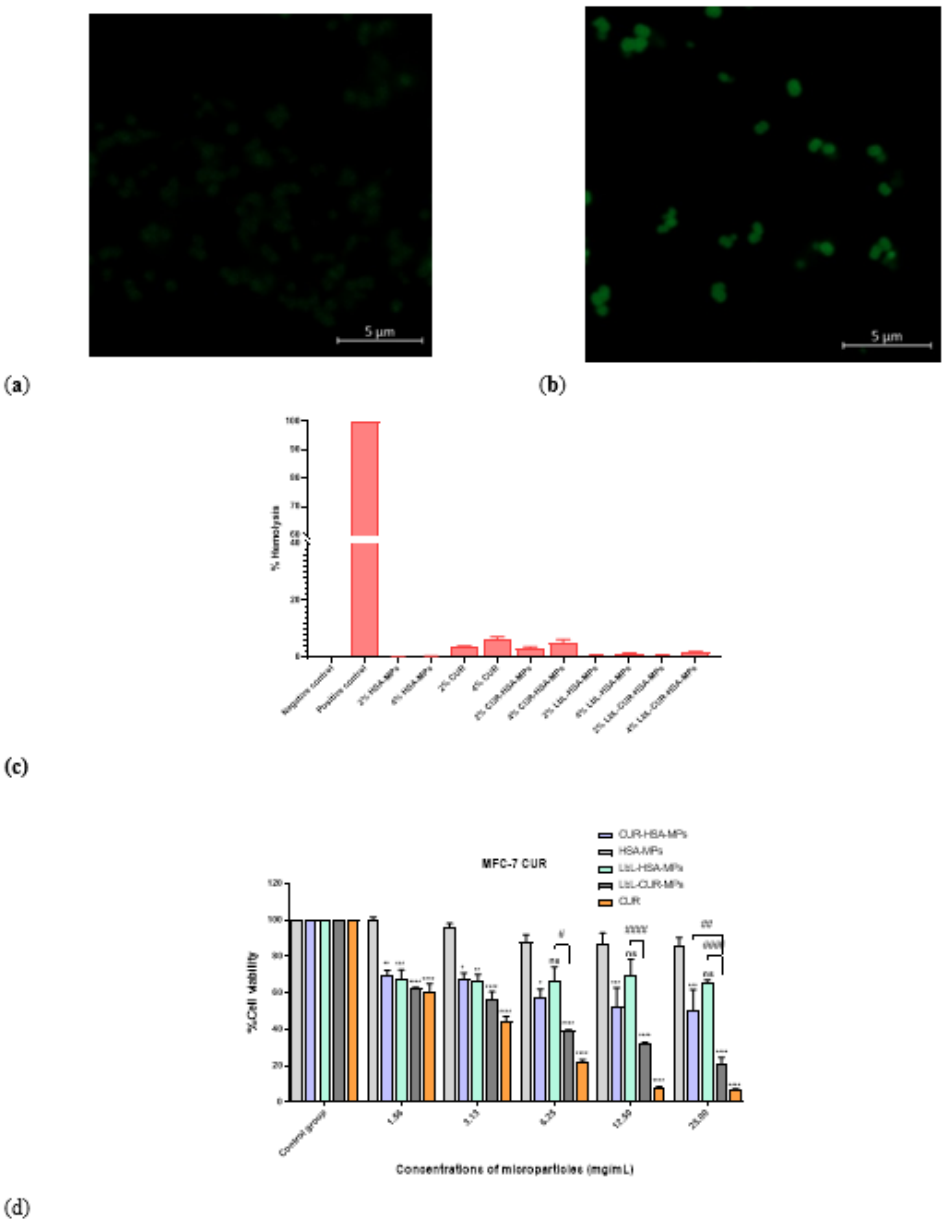


Figure 7 Confocal microscopy of (a) LbL-HSA-MPs and (b) LbL-CUR-loaded HSA-MPs. (c) Hemolysis analysis of free curcumin and MPs (n = 3). (d) Cytotoxicity effect of the polyelectrolyte MPs encapsulated with CUR on MCF-7 cells after 24 h of incubation (n=3). Values are expressed as mean ± standard error of the mean. *$p < 0.05$, **$p < 0.01$, ***$p < 0.001$, and ****$p < 0.0001$ were statistically significant values analyzed by two-way ANOVA compared to control group. $^{\#}p < 0.05$, $^{\#\#}p < 0.01$, $^{\#\#\#}p < 0.001$, and $^{\#\#\#\#}p < 0.0001$ were statistically significant values analyzed by two-way ANOVA

Hemolysis can be used to evaluate the biocompatibility of biomaterials. The hemolysis activities of CUR, HSA-MPs, CUR-MPs, LbL-HSA-MPs, and LbL-CUR-MPs are shown in **Figure 7(c)**. According to ISO 10993-4:2017, materials with hemolysis ratios below 5% are considered

hemocompatible. In this study, the hemolysis ratios of all samples at of 2% (w/v) were below 5%, indicating good blood compatibility. In contrast, free CUR and CUR-MPs 4% (w/v) showed slightly higher hemolysis values of approximately 6.06% and 5.13%, respectively. Furthermore, LbL-CUR-MPs exhibited higher hemolysis than LbL-HSA-MPs because incorporatiing CUR slightly increased hemolytic interactions [41]. These results further suggest that LBL-CUR-MPs had better blood compatibility than CUR and CUR-MPs. The above results confirmed that LbL-HSA-MPs exhibit good blood compatibility and can serve as biocompatible carrier without causing obvious hemolysis. Similar findings have been reported by Xu *et al*., who demonstrated negligible hemolytic activity of platelet membrane-encapsulated CUR NPs across a wide concentration range, further supporting the blood compatibility of polymeric CUR delivery systems [42].

The cell cytotoxicity of CUR-MPs and LBL-CUR-MPs revealed a concentration-dependent reduction in cell viability as the concentration increased from 1.56 to 25 mg/mL (**Figure 7(d)**). Notably, LbL-CUR-MPs exhibited greater cytotoxicity towards MCF-7 cells compared to CUR-HSA-MPs at all tested concentrations, although the differences were not statistically significant at concentrations up to 12.5 mg/mL. A significant reduction in cell viability was observed at 25 mg/mL ($p < 0.01$), indicating enhanced antiproliferative activity of the multilayer-coated formulation at higher concentrations. In this study, CUR-MPs reduced MCF-7 cell viability in a concentration-dependent manner, consistent with our prior findings that CUR-MPs have a dose-dependent cytotoxic effect on breast cancer cells [20]. Free CUR exhibited even higher cytotoxicity at this concentration due to its immediate bioavailability, indicating its potent anti-cancer effects. In contrast, unloaded LbL-HSA-MPs maintained significantly higher cell viability than LbL-CUR-MPs at concentrations ≥ 6.25 mg/mL ($p < 0.05$), indicating that the observed antiproliferative activity was primarily associated with CUR loading rather than the carrier system itself.

These results suggest that LbL-CUR-MPs are more effective in reducing MCF-7 cell viability than CUR-MPs, highlighting their potential as a superior delivery system for CUR in cancer therapy. The enhanced antiproliferative activity of CUR-loaded LbL-HSA-MPs compared with CUR-HSA-MPs may be associated with the presence of the PEI/ALG multilayer shell. PEI-containing systems are known to promote cellular interaction and internalization due to their cationic surface properties, which facilitate electrostatic interactions with negatively charged cell membranes [43]. Meanwhile, the ALG outer layer may partially shield the excessive positive charge of PEI, improving biocompatibility while maintaining efficient cellular uptake [44]. In addition, the multilayer coating may help retard the rapid diffusion of CUR from the MPs, prolonging the interaction between CUR and cancer cells. Similar observations have been reported in previous studies, showing that LbL polymer coatings can improve cellular uptake and sustain drug-release behavior in polymeric delivery systems [45].

The current study found that CUR-MPs and LbL-CUR-MPs were less cytotoxic than pure CUR in a dose- and time-dependent manner, suggesting that the polymer-based particles mitigate the cytotoxic effects of CUR. This aligns with previous research showing reduced cytotoxicity of CUR-chitosan NPs compared to the free drug, due to delayed drug release and steric hindrance. The covalent attachment of the drug to the polymer likely delays its immediate action, as the NPs act as intracellular depots, releasing the drug more slowly [46]. This could explain the observed delayed increase in toxicity. In a study involving CUR-loaded folate-modified chitosan NPs, a significant decrease in MCF-7 cell viability was observed as incubation time increased [47]. The cytotoxicity of CUR-loaded NPs was slightly higher than that of pure drugs after 7 days. Additionally, a previous study found that CUR-nanosuspensions with larger particle sizes were more effective in killing cancer cells after prolonged incubation [48]. These findings support the hypothesis that multilayer-coated MPs may prolong CUR–cell interactions and improve therapeutic performance over time. Further studies should evaluate long-term cytotoxicity, for example, with a 72-hour incubation, to explore the time-dependent effects of CUR-loaded MPs on MCF-7 cells. Assessing cell viability at various time points would provide valuable insights into the kinetics of CUR release and its sustained impact on cell viability.

A key limitation of this study is the inability to conduct a dose-response analysis beyond 25 mg/mL. At higher concentrations, excessive particle coverage of

cells may lead to cell death due to mechanical effects rather than CUR cytotoxicity, hindering accurate assessment of the true cytotoxic potential. Future studies should address this by optimizing particle size or concentration to allow for a more precise evaluation of the dose-response relationship. Furthermore, direct evaluation of *in vitro* release kinetics under physiological conditions and analyses of CUR stability were not performed in this work. Such analysis would provide deeper mechanistic insight into drug release behavior. Therefore, future studies should investigate the release kinetics and long-term stability of CUR-loaded LbL-HSA-MPs to further elucidate their therapeutic potential.

Cellular uptake of polyelectrolyte MPs

In **Figure 8**, the green fluorescence from the LbL-HSA-MPs is due to their uptake. The z-stack section for FITC-CUR-MPs, shown in **Figure 7(c)**, indicates that LBL-CUR-MPs were readily taken up by MCF-7 cells, likely via endocytosis pathways, including phagocytosis and macropinocytosis [49]. PEI-based systems tended to enter cells through caveolae-mediated endocytosis or micro-pinocytosis [38]. A PEI coating can assist cellular uptake to varying degrees among different cell types, as demonstrated by Patiño *et al*. [50]. Functionalization, whether intended or inherent, may influence the interaction of such particles with cellular membranes and potentially activate cellular internalization mechanisms. Compared with our previous CUR-HSA-MPs system, the present multilayer-coated MPs demonstrated improved biocompatibility and enhanced antiproliferative activity by incorporating PEI and ALG as functional coating layers. The LbL assembly strategy may enhance particle–cell interactions while partially reducing the inherent cytotoxicity associated with free PEI, highlighting the advantage of multilayer surface engineering for CUR delivery applications [44]. Nevertheless, further studies are needed to improve the biological properties and cellular uptake of MPs, as well as to understand their precise biological effects to optimize their use in cancer therapy.

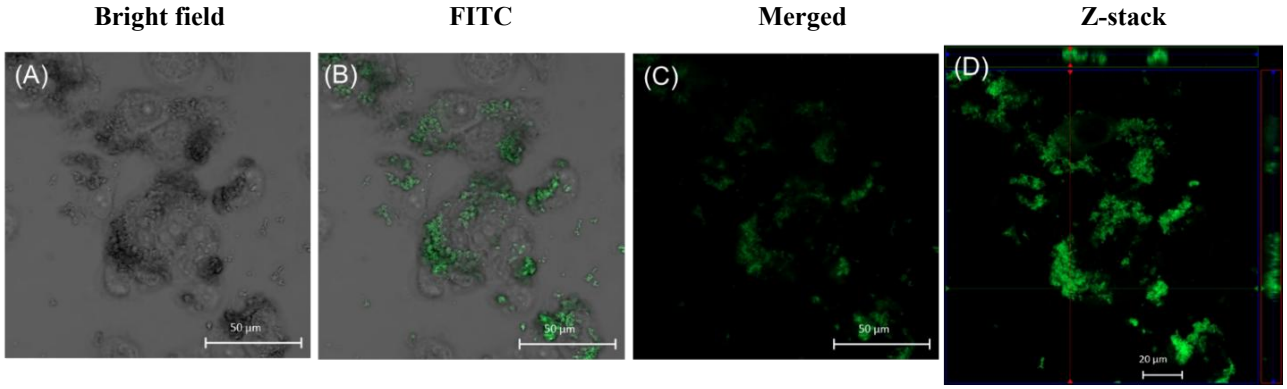


Figure 8 Cellular uptake of polyelectrolyte MPs. (a) bright field, (b) merge, (c) FITC, and (d) representative confocal z-stack images revealing cellular uptake of LbL-CUR-HSA-MPs (equivalent to 25 mg/mL of CUR) by MCF-7 cells after 4 h incubation.

Conclusions

This study has demonstrated that LbL-CUR-MPs prepared via electrostatic assembly of proper polymer building blocks offer sustained drug delivery. LBL-HSA-MPs were obtained, demonstrating significantly higher uptake by cancer cells than CUR-MPs. LbL-CUR-MPs generated after potential PEI shedding exhibited higher cytotoxicity compared to CUR-MPs, further emphasizing the therapeutic potential of the entire microcarrier system. These LbL-CUR-MPs exhibited good biocompatibility and excellent CUR loading capacity. Most importantly, the LbL-CUR-MPs exhibited the strongest antitumor efficacy compared with CUR-MPs alone *in vitro*. The results indicate that neutralization of PEI surface charge increases biocompatibility and enhances cell internalization efficiency. This makes biodegradable LbL-HSA-MPs a promising system for combined drug treatment in

efficient cancer therapy. However, future work should focus on *in vivo* evaluation, long-term stability assessment, release kinetics, and scalability to fully establish their clinical potential. Further animal models analyses will also be important to better understand particle properties.

Acknowledgements

This research was funded by the University of Phayao and Thailand Science Research and Innovation Fund (Grant No. FF65-RIM116), the School of Medical Sciences, University of Phayao, Thailand, (Grants No. MS 251001), and the Center of Excellence on Biodiversity, Ministry of Higher Education, Science, Research and Innovation, Thailand (Grant No. BDC-PG4-161012).

Declaration of Generative AI in Scientific Writing

The authors acknowledge the use of generative AI tools (e.g., QuillBot and ChatGPT by OpenAI) in the preparation of this manuscript, specifically for language editing and grammar correction. No content generation or data interpretation was performed by AI. The authors take full responsibility for the content and conclusions of the publication.

CRediT Author Statement

Surisak Prasarnpun: Conceptualization; Validation: Formal analysis; Resources; Writing - Review & Editing; Funding acquisition. **Netsai Sriaksor**: Methodology; Investigation. **Krissana Khoothiam**: Validation; Data Curation; Resources. **Nares khamcharoen**: Software. **Chonthida Thephinlap**: Validation; Data Curation. **Chutamas Thepmalee**: Software: Formal analysis; Resources. **Nittiya Suwannasom**: Conceptualization: Validation; Formal analysis; Investigation; Resources; Writing - Original Draft; Supervision.

References

[1] A Srivastava and A Prajapati. Albumin and functionalized albumin nanoparticles: Production strategies, characterization, and target indications. *Asian Biomedicine* 2020; **14(6)**, 217-242.

[2] M Madej, N Kurowska and B Strzalka-Mrozik. Polymeric Nanoparticles—tools in a drug delivery system in selected cancer therapies. *Applied Sciences* 2022; **12(19)**, 9479.

[3] N Salari, F Faraji, FM Torghabeh, F Faraji, K Mansouri, F Abam, S Shohaimi, H Akbari and M Mohammadi. Polymer-based drug delivery systems for anticancer drugs: A systematic review. *Cancer Treatment and Research Communications* 2022; **32**, 100605.

[4] S Maiolino, A Russo, V Pagliara, C Conte, F Ungaro, G Russo and F Quaglia. Biodegradable nanoparticles sequentially decorated with Polyethyleneimine and Hyaluronan for the targeted delivery of docetaxel to airway cancer cells. *Journal Nanobiotechnology* 2015; **13**, 29.

[5] C Maneerattanarungroj, P Lopin, C Khonthun, P Jaikhor and S Prasarnpun. Curcumin delivery using novel chitosan-polyethylene glycol diacrylate microencapsulation prepared via radiation-induced crosslinking. *Journal of Applied Pharmaceutical Science* 2022; **12(12)**, 021-030.

[6] A Spada, J Emami, JA Tuszynski and A Lavasanifar. The uniqueness of albumin as a carrier in nanodrug delivery. *Molecular Pharmaceutics* 2021; **18(5)**, 1862-1894.

[7] H Cho, SI Jeon, CH Ahn, MK Shim and K Kim. Emerging albumin-binding anticancer drugs for tumor-targeted drug delivery: Current understandings and clinical translation. *Pharmaceutics* 2022; **14(4)**, 728.

[8] L Meng, Y Cheng, S Gan, Z Zhang, X Tong, L Xu, X Jiang, Y Zhu, J Wu, A Yuan and Y Hu. Facile deposition of manganese dioxide to albumin-bound paclitaxel nanoparticles for modulation of hypoxic tumor microenvironment to improve chemoradiation therapy. *Molecular Pharmacology* 2018; **15(2)**, 447-457.

[9] W Shi, X Wan, Y Wang, J He, X Huang, Y Xu, W Zhang, R Chen, LWang, R Zheng, L Ma, X Li, L Xu, X Zha and J Wang. Nanoparticle albumin-bound paclitaxel-based neoadjuvant regimen: A promising treatment option for HER2-low-positive breast cancer. *Nanomedicine* 2023; **49**, 102666.

[10] N Suwannasom, N Sriaksorn, C Thepmalee, C Thephinlap, P Tanamatayarat, K Khoothiam, H Bäuemler and N Na-Ek. Efficacy and safety of nanoparticle albumin-bound paclitaxel in

advanced non-small cell lung cancer: A systematic review and meta-analysis of clinical trials and observational studies. *Heliyon* 2023; **9(11)**, e21903.

[11] SI Motegi, M Ishikawa, A Sekiguchi and O Ishikawa. Nanoparticle albumin-bound paclitaxel-and/or gemcitabine-induced scleroderma accompanied by acanthosis nigricans-like skin changes. *Case Reports in Dermatological Medicine* 2019; **11(3)**, 273-277.

[12] P Shende, A Patil and B Prabhakar. Layer-by-layer technique for enhancing physicochemical properties of actives. *Journal of Drug Delivery Science and Technology* 2020; **56(A)**, 101519.

[13] A Ismail and SF Chou. Polyethylenimine carriers for drug and gene delivery. *Polymers* 2025; **17(15)**, 2150.

[14] L Yang, J Guo, S Zhang and Y Gong. Preparation and characterization of novel super-artificial hair fiber based on biomass materials. *International Journal of Biological Macromolecules* 2017; **99**, 166-172.

[15] M Salehi, Z Bagher, SK Kamrava, A Ehterami, R Alizadeh, M Farhadi, M Falah and A Komeili. Alginate/chitosan hydrogel containing olfactory ectomesenchymal stem cells for sciatic nerve tissue engineering. *Journal of Cellular Physiology* 2019; **234(9)**, 15357-15368.

[16] A Ediriwickrema, J Zhou, Y Deng and W Saltzman. Multi-layered nanoparticles for combination gene and drug delivery to tumors. *Biomaterials* 2014; **35(34)**, 9343-9354.

[17] T Stylianopoulos, K Soteriou, D Fukumura and RK Jain. Cationic nanoparticles have superior transvascular flux into solid tumors: Insights from a mathematical model. *Annals of Biomedical Engineering* 2013; **41(1)**, 68-77.

[18] R Tutuianu, LM Popescu, MB Preda, AM Rosca, RM Piticescu and A Burlacu. Evaluation of the ability of nanostructured PEI-coated iron oxide nanoparticles to incorporate cisplatin during synthesis. *Nanomaterials* 2017; **7(10)**, 314.

[19] P Zhang, D Chen, L Li and K Sun. Charge reversal nano-systems for tumor therapy. *Journal of Nanobiotechnology* 2022; **20(1)**, 31.

[20] N Suwannasom, N Sriaksorn, C Thepmalee, K Khoothiam, A Prapan, H Bäumler and C Thephinlap. Curcumin-loaded albumin submicron particles with potential as a cancer therapy: An *in vitro* study. *Beilstein Journal of Nanotechnology* 2023; **14**, 1127-1140.

[21] S Chaiwaree, A Prapan, N Suwannasom, T Laporte, T Neumann, A Pruß, R Georgieva and H Bäumler. Doxorubicin–loaded human serum albumin submicron particles: Preparation, characterization and *in vitro* cellular uptake. *Pharmaceutics* 2020; **12(3)**, 224.

[22] M Jäger, S Schubert, S Ochrimenko, D Fischer and US Schubert. Branched and linear poly(ethylene imine)-based conjugates: Synthetic modification, characterization, and application. *Chemical Society Reviews* 2012; **41(13)**, 4755-4767.

[23] GB Ding, X Meng, P Yang, B Li, RH Stauber and Z Li. Integration of polylactide into polyethylenimine facilitates the safe and effective intracellular siRNA delivery. *Polymers* 2020; **12(2)**, 445.

[24] P Trosan, JSJ Tang, RR Rosencrantz, L Daehne, AD Smaczniak, S Staehlke, S Chea and TA Fuchsluger. The biocompatibility analysis of artificial mucin-like glycopolymers. *International Journal of Molecular* 2023; **24(18)**, 14150.

[25] K Yu, J Zhao, C Yu, F Sun, Y Liu, Y Zhang, RJ Lee, L Teng and Y Li. Role of four different kinds of polyethylenimines (PEIs) in preparation of polymeric lipid nanoparticles and their anticancer activity study. *Journal of Cancer* 2016; **7(7)**, 872-882.

[26] V Kafil and Y Omidi. Cytotoxic impacts of linear and branched polyethylenimine nanostructures in A431 cells. *BioImpacts* 2011; **1(1)**, 23-30.

[27] L Gholami, HR Sadeghnia, M Darroudi and RK Oskuee. Evaluation of genotoxicity and cytotoxicity induced by different molecular weights of polyethylenimine/DNA nanoparticles. *Turkish Journal of Biology* 2014; **38(3)**, 380-387.

[28] E Naumenko, F Akhatova, E Rozhina and R Fakhrullin. Revisiting the cytotoxicity of cationic polyelectrolytes as a principal component in layer-by-layer assembly fabrication. *Pharmaceutics* 2021; **13(8)**, 1230.

[29] J Wang, Y Hu, Y Han, Q Fang, Z Chen, Y Wang, P Zhao, H Wang and Q Lin. Non-viral gene coating modified IOL delivering PDGFR-α

shRNA interferes with the fibrogenic process to prevent posterior capsular opacification. *Regen Biomaterials* 2023; **10**, rbad020.

[30] K Jantakee, A Prapan, S Chaiwaree, N Suwannasom, W Kaewprayoon, R Georgieva, Y Tragoolpua and H Bäumler. Fabrication and characterization of human serum albumin particles loaded with non-sericin extract obtained from silk cocoon as a carrier system for hydrophobic substances. *Polymers* 2021; **13(3)**, 334.

[31] N Suwannasom, K Smuda, C Kloypan, W Kaewprayoon, N Baisaeng, A Prapan, S Chaiwaree, R Georgieva, H Bäumler. Albumin submicron particles with entrapped riboflavin-fabrication and characterization. *Nanomaterials* 2019; **9(3)**, 482.

[32] DS Kolotova, EV Borovinskaya, VV Bordiyan, YF Zuev, VV Salnikov, OS Zueva and SR Derkach. Phase behavior of aqueous mixtures of sodium alginate with fish gelatin: Effects of pH and ionic strength. *Polymers* 2023; **15(10)**, 2253.

[33] Z Benmamoun, T Kinard, P Chandar, J Jankolovits and WA Ducker. Effect of salt on synthetic cationic antimicrobial polymer-cell interactions. *Biomacromolecules* 2025; **26(6)**, 3322-3330.

[34] L Riva, A Fiorati and C Punta. Synthesis and application of cellulose-polyethyleneimine composites and nanocomposites: A concise review. *Materials* 2021; **14(3)**, 473.

[35] A Zakeri, MAJ Kouhbanani, N Beheshtkhoo, V Beigi, SM Mousavi, SAR Hashemi, AK Zade, AM Amani, A Savardashtaki, E Mirzaei, S Jahandideh and A Movahedpour. Polyethylenimine-based nanocarriers in co-delivery of drug and gene: A developing horizon. *Nano Reviews & Experiments* 2018; **9(1)**, 1488497.

[36] S Shahapurmath, BR Sharannavar and R Koli. Serum albumin nanoparticles: Ligand functionalization for enhanced targeted therapeutics in precision medicine. *Medicine in Drug Discovery* 2025; **27**, 100218.

[37] A Kumar, SS Das, S Tambe, B Kaundal, SK Sarraf and KK Kesari. Unravelling the potential role of polyethyleneimine (PEI)-based nanosystems in skin cancer therapy. *Materials Advances* 2024; **6(2)**, 490-507.

[38] B Singh, S Maharjan, TE Park, T Jiang, SK Kang, YJ Choi and CS Cho. Tuning the buffering capacity of polyethylenimine with glycerol molecules for efficient gene delivery: Staying in or out of the endosomes. *Macromolecular Bioscience* 2015; **15(5)**, 622-635.

[39] HW Chen, SD Chen, HT Wu, CH Cheng, S Chiou and WT Chen. Improvement in Curcumin's stability and release by formulation in flexible Nano-liposomes. *Nanomaterials* 2024; **14(22)**, 1836.

[40] D Hudiyanti, MFA Khafiz, K Anam, P Siahaan and SM Christa. *In vitro* evaluation of curcumin encapsulation in gum arabic dispersions under different environments. *Molecules* 2022; **27(12)**, 3855.

[41] V Krishnan, GD Venkatasubbu and T Kalaivani. Investigation of hemolysis and antibacterial analysis of curcumin-loaded mesoporous SiO2 nanoparticles. *Applied Nanoscience* 2023; **13(1)**, 811-888.

[42] L Xu, Y Zhou, N Li, A Yang and H Qi. Platelet membrane encapsulated curcumin nanomaterial-mediated specific thrombolysis and anti-thrombotic treatment among pregnant women. *Biomaterials Science* 2024; **12(12)**, 3163-3174.

[43] W Li, X Lei, H Feng, B Li, J Kong and M Xing. Layer-by-Layer cell encapsulation for drug delivery: The history, technique basis, and applications. *Pharmaceutics* 2022; **14(2)**, 297.

[44] Y Chen, C Liu, Z Yang, Y Sun, X Chen and L Liu. Fabrication of zein-based hydrophilic nanoparticles for efficient gene delivery by layer-by-layer assembly. *International Journal of Biological Macromolecules* 2022; **217**, 381-397.

[45] W Sun, X Zhang, HR Jia, YX Zhu, Y Guo, G Gao, YH Li and FG Wu. Water-dispersible candle Soot–derived carbon nano-onion clusters for imaging-guided photothermal cancer therapy. *Small* 2019; **15(11)**, e1804575.

[46] SW Ng, GT Selvarajah, MZ Hussein, SK Yeap and AR Omar. *In vitro* evaluation of curcumin-encapsulated chitosan nanoparticles against feline infectious peritonitis virus and pharmacokinetics study in cats. *BioMed Research International* 2020; **2020**, 3012198.

[47] S Esfandiarpour-Boroujeni, S Bagheri-Khoulenjani, H Mirzadeh and S Amanpour. Fabrication and study of curcumin loaded nanoparticles based on folate-chitosan for breast cancer therapy application. *Carbohydrate Polymers* 2017; **168**, 14-21.

[48] C Bi, XQ Miao, SF Chow, WJ Wu, R Yan, YH Liao, AHL Chow and Y Zheng. Particle size effect of curcumin nanosuspensions on cytotoxicity, cellular internalization, *in vivo* pharmacokinetics and biodistribution. *Nanomedicine* 2017; **13(3)**, 943-953.

[49] K El-Boubbou, R Ali, H Al-Zahrani, T Trivilegio, AH Alanazi, AL Khan, M Boudjelal and A AlKushi. Preparation of iron oxide mesoporous magnetic microparticles as novel multidrug carriers for synergistic anticancer therapy and deep tumor penetration. *Scientific Reports* 2019; **9(1)**, 9481.

[50] T Patiño, J Soriano, L Barrios, E Ibáñez and C Nogués. Surface modification of microparticles causes differential uptake responses in normal and tumoral human breast epithelial cells. *Scientific Reports* 2015; **5(1)**, 11371.